Front. Earth Sci. 2018, 12(1): 24–36
https://doi.org/10.1007/s11707-017-0631-6

RESEARCH ARTICLE

Seasonal variation of the global mixed layer depth: comparison between Argo data and FIO-ESM

Yutong ZHANG[1], Haiming XU (✉)[1], Fangli QIAO[3], Changming DONG (✉)[2]

1 College of Atmospheric Sciences, Nanjing University of Information Science and Technology, Nanjing 210044, China
2 College of Marine Sciences, Nanjing University of Information Science and Technology, Nanjing 210044, China
3 First Institute of Oceanography, State Oceanic Administration, Qingdao 266061, China

Abstract The present study evaluates a simulation of the global ocean mixed layer depth (MLD) using the First Institute of Oceanography-Earth System Model (FIO-ESM). The seasonal variation of the global MLD from the FIO-ESM simulation is compared to Argo observational data. The Argo data show that the global ocean MLD has a strong seasonal variation with a deep MLD in winter and a shallow MLD in summer, while the spring and fall seasons act as transitional periods. Overall, the FIO-ESM simulation accurately captures the seasonal variation in MLD in most areas. It exhibits a better performance during summer and fall than during winter and spring. The simulated MLD in the Southern Hemisphere is much closer to observations than that in the Northern Hemisphere. In general, the simulated MLD over the South Atlantic Ocean matches the observation best among the six areas. Additionally, the model slightly underestimates the MLD in parts of the North Atlantic Ocean, and slightly overestimates the MLD over the other ocean basins.

Keywords mixed layer depth, FIO-ESM model, seasonal variation

1 Introduction

A surface mixed layer (ML) exists in the ocean where temperature, salinity and density are nearly uniform in the vertical direction. The surface ML plays an important role in air-sea interaction. The air-sea energy and material exchanges are mainly conducted through the ML. The mixed layer depth (MLD) varies greatly with time, which partially reflects oceanic responses to atmospheric forcing (Perry and Walker, 1977; de Boyer Montégut et al., 2004). Climate researchers are interested in MLD since its variation is one of the major factors controlling sea surface temperature (SST) (Deser et al., 1996). Marine biologists are interested in ML variations because they can directly affect primary production (Alexander et al., 2001; Ohno et al., 2009). There are different ways to define the MLD. One method is to use temperature difference, such as using a temperature difference of 0.1°C–1.0°C with respect to the SST (Sprintall and Roemmich, 1999). The second method is to use a density difference of 0.01–0.10 kg/m^3 with respect to the density at the surface (Sprintall and Tomczak, 1992; Kelly and Bo, 1995). The third method is to use a gradient, that is, the depth at which temperature gradient or density gradient exceeds a threshold; for example, some studies used a potential-density gradient criterion of 0.0005 kg·m^{-3}·dbar^{-1} or a temperature gradient criterion of 0.005°C·dbar^{-1} (Kara et al., 2000; Thomson and Fine, 2010). The fourth method is a hybrid method which takes the general shape of the MLD from each ocean profile, finds physical features of the profile, and assembles a suite of appropriate MLD values by calculating threshold MLD and gradient MLD (Holte and Talley, 2009).

In recent years, many studies focused on the importance of MLD variability in terms of air-sea interaction. An et al. (2012) calculated the global MLD, and analyzed its temporal and spatial variation. They showed that the distribution and change of the MLD are similar in the North Pacific Ocean and the North Atlantic Ocean, while those in the Indian Ocean are different, mainly influenced by monsoons. Lu et al. (2008) used Argo and Levitus data to compute the MLD and investigated the distribution of the MLD in summer. They found that in the latitudes of 20°S–20°N and 40°–60°S, the MLD calculated from the Levitus data was smaller than that calculated from the Argo data; in the latitudes of 40°–60°N, the MLD calculated from the Levitus data was only slightly smaller

Received July 7, 2016; accepted November 21, 2016

E-mail: hxu@nuist.edu.cn (Haiming XU), cmdong@gmail.com (Changming DONG)

than that from the Argo data. In the latitudes of 20°–40°N and 20°–40°S where the MLD is smaller and in the oceanic areas poleward of 60°N or 60°S, the differences of the MLD calculated by the two datasets are small. Ohno et al. (2009) estimated the monthly-mean climatology of the MLD in the North Pacific in terms of Argo observations; they revealed for the first time that there were two bands of deep ML with depths greater than 200 m north and south of the Kuroshio Extension in winter. Kolodziejczyk et al. (2015) studied the inter-annual variability of winter convection in the ML in the subtropical North Atlantic Ocean. They suggested that inter-annual variability of the mixing winter convection driven by atmospheric buoyancy flux can generate inter-annual variability of MLD in late winter. Regarding the ML formation mechanisms, previously it was believed that the turbulent mixing associated with wind stress stirring and surface buoyancy forcing played key roles. Sea surface heat fluxes, momentum flux, and freshwater flux are the essential factors for MLD formation in the one-dimensional ML model by Price et al. (1986). Recently, Qiao et al. (2008, 2013) found that sea surface waves have an important effect on the formation of the ML, and the wave-induced mixing penetration depth can reach nearly 100 m in the high latitudes and 30 m in the tropical oceans. Numerical experiments excluding shear induced vertical mixing clearly indicate that the non-breaking surface wave-induced mixing is responsible for the formation of the summer ML, while surface cooling-induced surface buoyancy forcing is responsible for the formation of the winter ML (Qiao and Huang, 2012).

Due to the importance of the MLD, accurate data for estimating MLD are indispensable for climate modeling, prediction, and research. Since the Argo observational data is only available over a short period, a long-term and basin-scale MLD dataset is needed. A global climate model is an important tool to predict seasonal and inter-annual variation in the MLD, with significant impact on the development of air-sea coupled models. Kara et al. (2000, 2003) analyzed inter-annual variability of SST and MLD in a systematic way for model-data comparison; their results revealed that 6-hourly wind and thermal forcing products were sufficiently accurate to simulate SST and MLD in an oceanic general circulation model (OGCM), in comparison to daily buoy time series. Noh and Lee (2008) compared the MLD from an OGCM and that from the climatological World Ocean Atlas 2005 (WOA05) data; they found reasonable agreement between the two with biases smaller than 20 m in most regions, although larger differences were found in the regions of western boundary currents, the equatorial zones, and the high-latitude oceans.

Most OGCMs have overlooked the importance of surface waves, leading to an underestimation of MLD and an overestimation of SST due to insufficient vertical mixing, especially in summer (Martin, 1985; Kantha and Clayson, 1994; Ezer, 2000; Qiao et al., 2008). The present study uses the FIO-ESM developed by the First Institute of Oceanography, State Oceanic Administration, which includes the surface wave-induced vertical mixing. The inclusion of the wave-induced mixing makes the FIO-ESM different from all other climate system models participating in the Coupled Model Intercomparison Project Phase 5 (CMIP5) (Song et al., 2007; Qiao et al, 2013). Some studies have shown that climate models with surface waves can remarkably improve their performance, with better simulated cold tongues (Song et al., 2007) in the tropic Pacific Ocean, and with better simulated temperatures in the other ocean basins (Huang et al., 2008; Song et al., 2011). Qiao et al. (2004) showed that the wave-induced mixing is strong south of 30°S in summer and it is strong north of 30°N in the North Pacific and Atlantic oceans in winter, as well as in the Southern Oceans south of 40°S. Adding the vertical mixing coefficient associated with the waves to the vertical diffusivity in a global OGCM produced a temperature structure in the upper 100 m much closer to the observational data than without the wave-induced mixing. Present study assesses the performance of the global ocean MLD based on the FIO-ESM and focuses on its seasonal variation. Considering the influences of temperature and salinity, the MLD here is defined by the potential density threshold using the depth where potential density increases by 0.03 kg/m^3 from its value at 10 m. The choice for 10 m is based on the following two reasons: first, the upper layer in most ocean component models has a thickness of 10 m ; second, the reference depth is set at 10 m in order to reduce the local outlier induced by strong diurnal variation in the upper ocean (Huang et al. 2014). The choice for the 0.03 kg/m^3 threshold criterion was based on de Boyer Montégut et al. (2004). For each Argo profile, the MLD based on a range of different density criteria was computed. Analysis of these profiles shows that the 0.01 kg/m^3 threshold yields too shallow of a mixed layer for our purposes. A value of 0.1 kg/m^3 sometimes yielded the depth of the main thermocline, and a value of 0.05 kg/m^3 often falls within the seasonal thermocline rather than at its top (de Boyer Montégut et al., 2004). Therefore a threshold of 0.03 kg/m^3 may be the appropriate value for the density criterion here.

The rest of the paper is organized as follows. The data and methods are described in Section 2. We introduce the results of seasonal variation in the global ocean MLD by comparing FIO-ESM output and Argo observational data in Section 3. Summary and discussion are given in Section 4.

2 Data and method

2.1 Data

The coupled model includes the Community Atmospheric Model (CAM3; Collins et al., 2004), Surface Wave Model (MASNUM; Yang et al., 2005), OGCM (POP2.0; Smith et

al., 2010), Community Sea Ice Model (CICE4; Shu et al., 2013), and Comprehensive Land Surface Model (CLM3.5; Oleson et al., 2008). The POP model has a horizontal resolution of 1°×0.27° (latitude by longitude near the equator) to 1°×0.54° (high latitude) and a vertical coordinate of 40 levels. Different from other climate models, the FIO-ESM includes wave-induced mixing to better simulate the MLD by considering the non-breaking wave-related vertical mixing (Qiao et al., 2004).

The wave model obtains the wave number spectrum from the 10 m wind field produced by CAM3. Then, the vertical mixing coefficient B_V induced by the non-breaking wave from the wave model is added to the vertical eddy viscosity coefficient in the momentum equation, and to the vertical dissipation coefficient both in the temperature and salinity equations of OGCM. Thus, the total vertical mixing coefficient can be obtained as follows:

$$B_V = \alpha \iint_{\vec{k}} E\left(\vec{k}\right) \exp(2kz)\mathrm{d}\vec{k} \frac{\partial}{\partial z}\left[\iint_{\vec{k}} \omega^2 E\left(\vec{k}\right) \times \exp(2kz)\mathrm{d}\vec{k}\right]^{\frac{1}{2}}, \quad (1)$$

where α is a constant defined in the FIO-ESM model; $E\left(\vec{k}\right)$ is the wave number spectrum, ω is the angular frequency of wave, k is the wave number; z denotes water depth, $z = 0$ is the sea level, and the upward direction is defined as positive.

The coupling frequency is one hour with the CICE4; six hours with MASNUM, POP, and CAM3; and 24 hours with the CLM3.5. The vertical mixing effect induced by surface waves is not applied to sea-ice areas (ice coverage rate larger than 50%) (Shu et al., 2013). Details regarding MASNUM can be found in Yang et al. (2005). The monthly-mean outputs from January 1992 to December 2013 are analyzed in this study.

The abundant data from Argo floats are a great force for the development of marine sciences, especially for oceanic ML research. The international Argo project was launched in 2000. It deploys over 3000 floats, allowing about 3°×3° spatial resolution in the global ocean to observe three-dimensional (3D) ocean structures in real time. The monthly observed Argo float profiles increased rapidly from 2004 to 2005, especially in the Indian Ocean. Due to sparse Argo float input from 1995 to 1999, only the observational data since 2000 are used in this study.

2.2 Method

2.2.1 MLD calculation

The potential density threshold of 0.03 kg/m^3 is used to calculate MLD both in the model and the observational data: the density difference between the surface (10 m) and the bottom of the MLD is 0.03 kg/m^3. Suppose that the densities in the two critical layers are ρ_1 and ρ_2, the depths are D_1 and D_2 , ML density is ρ_M and surface density is ρ_0. A linear interpolation between D_1 and D_2 is then used to estimate the exact depth at which the difference criterion is reached. According to Eq. (2):

$$MLD = (\rho_M - \rho_1) \cdot \left(\frac{D_2 - D_1}{\rho_2 - \rho_1}\right) + D_1, \quad (2)$$

$$\rho_M = \rho_0 + 0.03. \quad (3)$$

The specific calculation of the MLD can be found in the paper by Holte and Talley (2009) or visit "http://mixedlayer.ucsd.edu/" to find the program for calculating the MLD using Argo data from the University of California, San Diego.

2.2.2 Deviation, relative errors, and correlation coefficients

Deviation of model output from the observational data is defined as

$$D = \mathrm{MLD}_{(\mathrm{model})} - \mathrm{MLD}_{(\mathrm{observation})}. \quad (4)$$

Relative error is defined as

$$R = \frac{\mathrm{MLD}_{(\mathrm{model})} - \mathrm{MLD}_{(\mathrm{observation})}}{\mathrm{MLD}_{(\mathrm{mean})}} \times 100\%. \quad (5)$$

Correlation coefficient is defined as

$$r = \frac{\frac{1}{n}\sum_{i=1}^{n}(x_i - \overline{x})(y_i - \overline{y})}{\sqrt{\frac{1}{n}\sum_{i=1}^{n}(x_i - \overline{x})^2}\sqrt{\frac{1}{n}\sum_{i=1}^{n}(y_i - \overline{y})^2}}. \quad (6)$$

3 Results

Figure 1 compares the simulated annual-mean MLD with the observations. The spatial distributions of MLD in these two datasets are quite similar. The ML is deeper in the Southern Hemisphere than in the Northern Hemisphere over the Pacific Ocean and the Indian Ocean, while the opposite is found in the Atlantic Ocean. In the Northern Hemisphere, the large MLD is mainly located in the northwest of the Atlantic Ocean. The model underestimates the MLD in comparison with the Argo observation in the northwest of the Atlantic Ocean. In the Southern Hemisphere, the difference between the simulated and observed MLD is small. The largest MLD extends from the West Indian Ocean to the eastern Pacific near 40°–60°S,

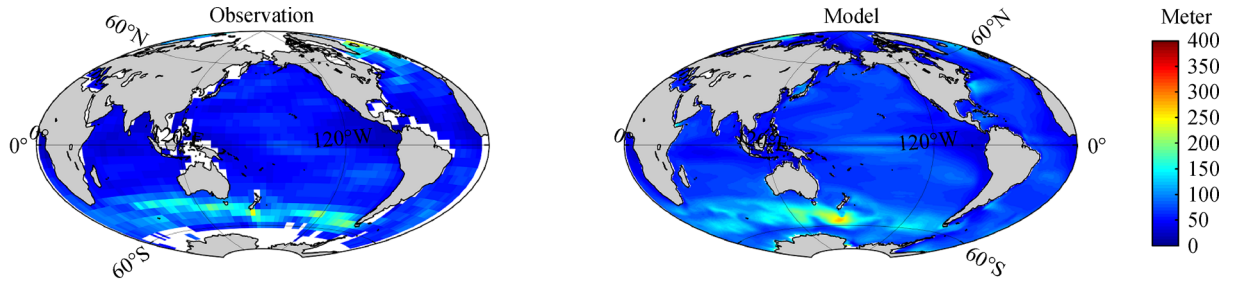

Fig. 1 Annual-mean MLD from FIO-ESM simulation and Argo data.

which is associated with the strong westerly wind over the Antarctic Circumpolar Current (ACC). Moreover, the MLD is smaller than 100 m south of 60°S due to freshwater injection from Antarctic continent.

3.1 Seasonal variation of MLD

Previous studies generally divided the global ocean into six sectors, namely the North Pacific Ocean, (100°E–70°W, 0°–60°N), the North Indian Ocean (24°–100°E, 0°–30°N), the North Atlantic Ocean (70°W–24°E, 0°–60°N), the South Pacific Ocean (120°E–70°W, 0°–60°S), the South Indian Ocean (24°–120°E, 0°–60°S), and the South Atlantic Ocean (70°W–24°E, 0°–60°S).

The seasons in the Northern Hemisphere are defined as spring (March to May, or MAM), summer (June to August, or JJA), fall (September to November, or SON), and winter (December to the following February, or DJF), which are the opposite in the Southern Hemisphere. As shown in Figs. 2 to 7, the MLD exhibits significant seasonal variation. Throughout all seasons, the MLD from the FIO-ESM is comparable to that from the Argo data. The simulated MLD is similar to the observational data with small deviations in five ocean basins: the North Pacific Ocean, the North Atlantic Ocean, the South Pacific Ocean, the South Indian Ocean, and the South Atlantic Ocean. It is largely overestimated over the North Indian Ocean; observed sea surface salinity is quite low, while the model results have much higher values. To quantify the model's performance in each ocean, spatial correlation coefficients between the observed and simulated MLD are given in Table 1. It can be clearly seen that the correlation coefficients exceed 0.6 for all six ocean basins. In the boreal summer, the spatial correlation coefficients exceed 0.85 in all basins. In the austral fall, the spatial coefficient is above 0.90 over the South Atlantic Ocean, indicating that the model can well reproduce the MLD in this region. In the boreal spring, the correlation coefficients are generally above 0.80, except for the North Atlantic Ocean and the North Indian Ocean. However, the correlation coefficients in the boreal winter are smaller than those in the boreal summer and fall over the North Atlantic Ocean and the Indian Ocean.

In the northern oceans (i.e., the North Pacific Ocean, the North Atlantic Ocean, and the North Indian Ocean), the MLD is deep in winter, shallow in summer, and gradually deepens during fall. As shown in Figs. 2 and 3, the MLD becomes shallow from 30°N to 60°N in the North Pacific Ocean and 15°N to 60°N in the North Atlantic Ocean during summer, showing similar patterns in both oceans. The simulated MLD agrees well with the observed one in most regions. During fall, the MLD increases gradually towards the north. Except for areas south of the Aleutian Islands, the simulated MLD is similar to the observation. In winter, the MLD is deep with its maximum value greater than 150 m north of 40°N over the strong western boundary current regions (the Gulf Stream and the Kuroshio). In comparison, the MLD in the North Pacific Ocean is shallower than that in the North Atlantic Ocean at the same latitudes due to the halocline developed by rainfall and the lower water upwelling (Kara et al., 2003). Meanwhile, the MLD is overestimated in the northeast of the Alaska Gulf (Fig. 2). In late winter, the maximum MLD exceeds 250 m over the North Atlantic Ocean. The simulated MLD shows a long narrow band of large value extending from the southwest (40°–80°W, 30°–45°N) to the northeast (10°–25°W, 40°–45°N), while smaller MLD occurs east of Newfoundland (Fig. 3). Compared with the observation, the simulated MLD is shallower in the east and deeper in the west of the North Atlantic Ocean, and the

Table 1 Spatial correlation coefficients between observed and simulated MLD in each season of each ocean basin

Season	North Pacific	North Atlantic	North Indian	South Atlantic	South Pacific	South Indian
Spring	0.81	0.68	0.65	0.85	0.80	0.84
Summer	0.87	0.85	0.85	0.84	0.70	0.71
Fall	0.81	0.83	0.71	0.90	0.74	0.87
Winter	0.80	0.61	0.62	0.89	0.81	0.86

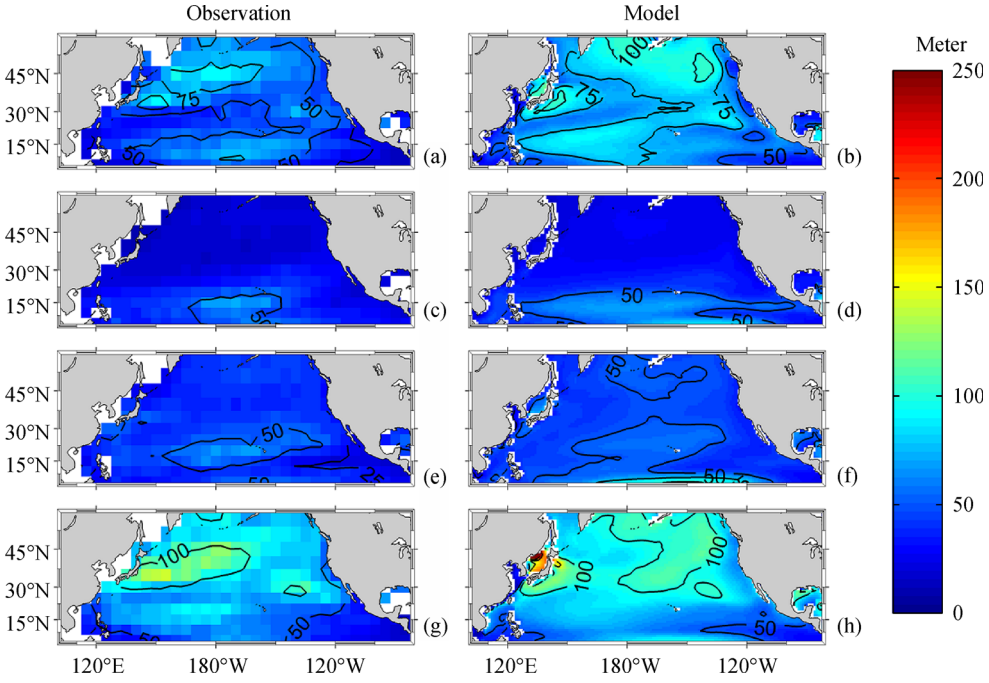

Fig. 2 Seasonal variation in MLD distribution in FIO-ESM simulation and Argo observation in the North Pacific Ocean (100°E–70°W, 0°–60°N) in four seasons: spring (a–b), summer (c–d), fall (e–f), and winter (g–h).

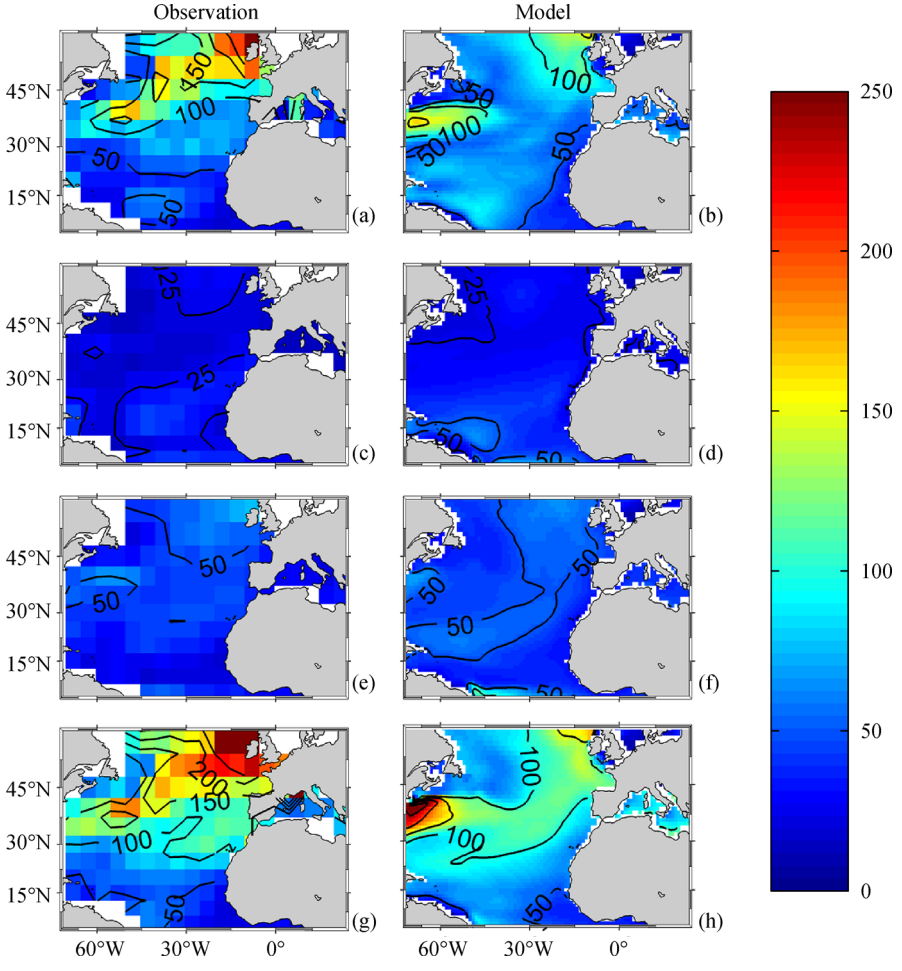

Fig. 3 Same as Fig. 2, except for the North Atlantic Ocean (70°W–24°E, 0°–60°N).

bias is small. In spring, the MLD becomes shallower, together with a narrow band of high values shifting northward. In the North Pacific Ocean, the MLD variation displays a meridional pattern of "deep-shallow-deep". The model approximately simulates the spatial distribution of MLD, in spite of some biases over the equator and at mid and high latitudes. In terms of the Atlantic, two evident transition regions in the west (40°–80°W, 30°–45°N,) and northeast (10°–25°W, 40°–45°N) are well captured in the model.

Geographical characteristics make the Indian Ocean unique with its typical monsoon climate. Figure 4 presents the seasonal variation of MLD in the North Indian Ocean, which is different from that in the North Pacific Ocean and North Atlantic Ocean. The semi-annual cycle feature is obvious in the Arabic Sea and the Bay of Bengal, with the deepest MLD in both summer and winter. Prasad (2004) examined the deep MLD in the North Indian Ocean during summer. The prevailing southwest monsoon in summer brings a strong heating effect from the Tibetan Plateau to the atmosphere; therefore, the wind stress forcing plays a dominant role in its MLD formation. The MLD in the Arabic Sea is evidently deeper than that in the Bay of Bengal, likely due to more freshwater entering into the bay. The simulated MLD in the Bay of Bengal is more than 20 m deeper than that in the observations in both spring and fall. In winter, the simulated value is generally comparable to the observation, and the MLD bias in the Bay of Bengal is lower than that in the Arabic Sea. The spatial correlation coefficient can reach 0.85 in summer and exceed 0.70 in spring and fall. Thus, the spatial distribution of simulated MLD is similar to the observation, exhibiting a remarkable semi-annual feature despite some overestimations in this region.

In the Southern Hemisphere, the observed MLD is also deep in winter and shallow in summer, and both spring and fall are deemed to be transitional seasons. The MLD in the southern oceans is mostly deeper than that in the northern oceans, with large (small) values in the subpolar (equatorial) regions throughout the longitude band. An et al. (2012) elucidated that the thermal expansion coefficient is small in high latitudes of the Southern Hemisphere, which results in the formation of the stable stratification. As shown in Fig. 5, the simulated MLD in the South Atlantic Ocean is quite consistent with the observation. The MLD is less than 100 m during summer. In March, a deep MLD band extends from the southwest to the north over the South Atlantic Ocean. The MLD reaches its maximum (250 m) in late austral winter and decreases after October. The simulation in this region is similar to the observational data, especially in summer with the annual-mean bias less than 5 m. These results are consistent with Huang et al. (2012), suggesting that the introduction of surface wave effectively improves the simulation in MLD over the South Atlantic Ocean. In Table 1, correlation coefficients over the South Atlantic Ocean are above 0.80 in the austral spring, summer, and fall. In the austral winter, the bias shows a meridional pattern of "positive-negative-

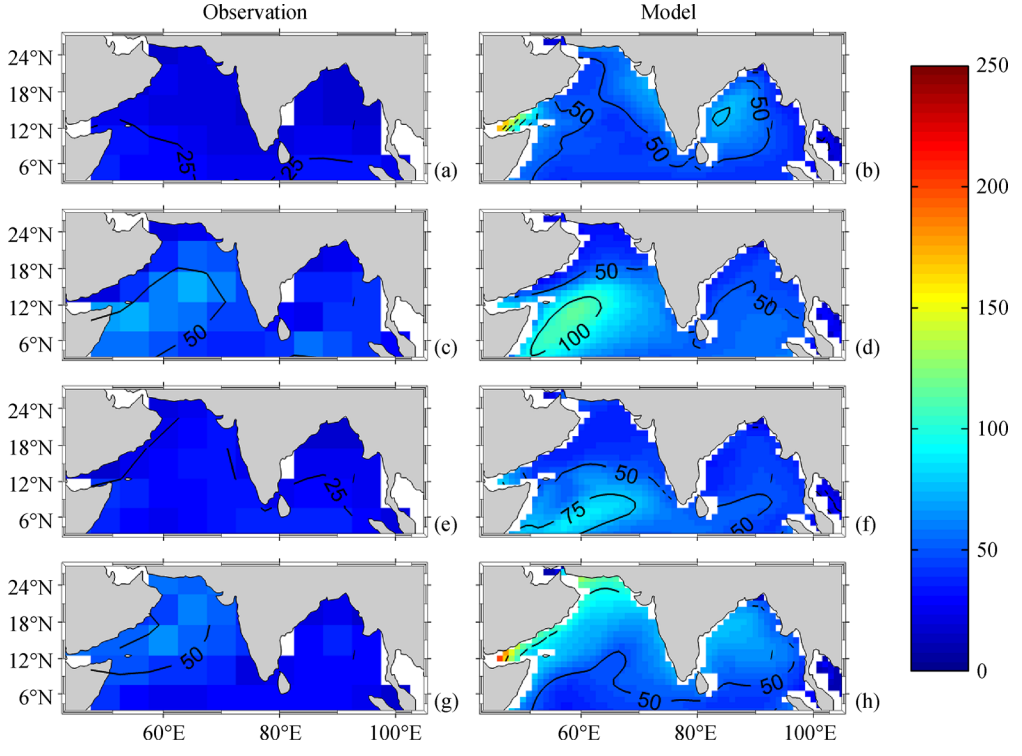

Fig. 4 Same as Fig. 2, except for the North Indian Ocean (24°–100°E, 0°–30°N).

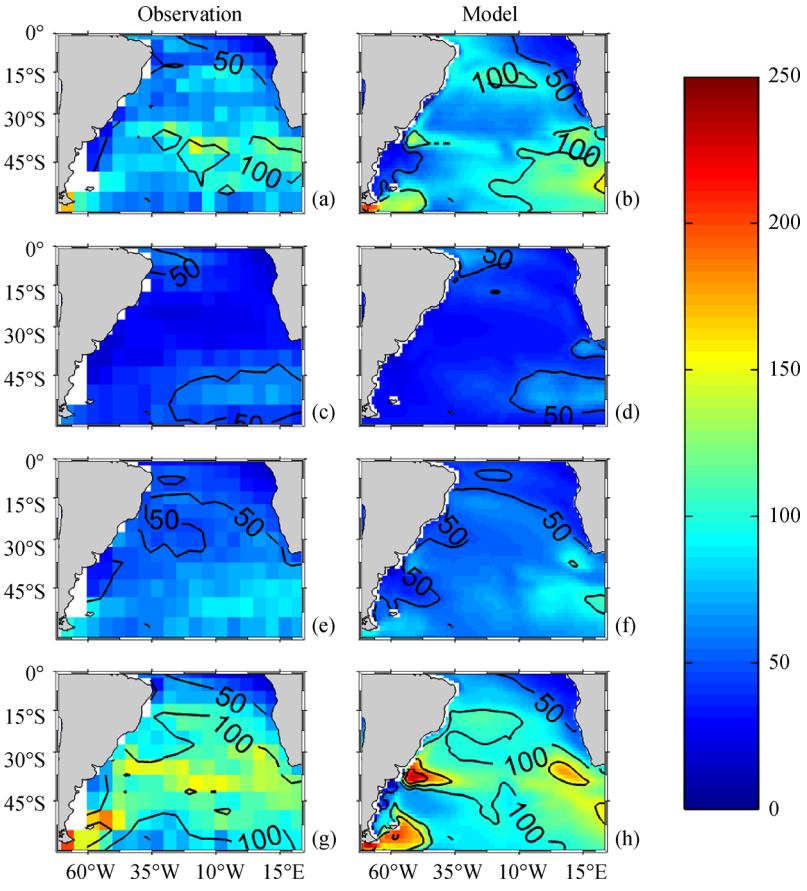

Fig. 5 Same as Fig. 2, except for the South Atlantic Ocean (70°W–24°E, 0°–60°S).

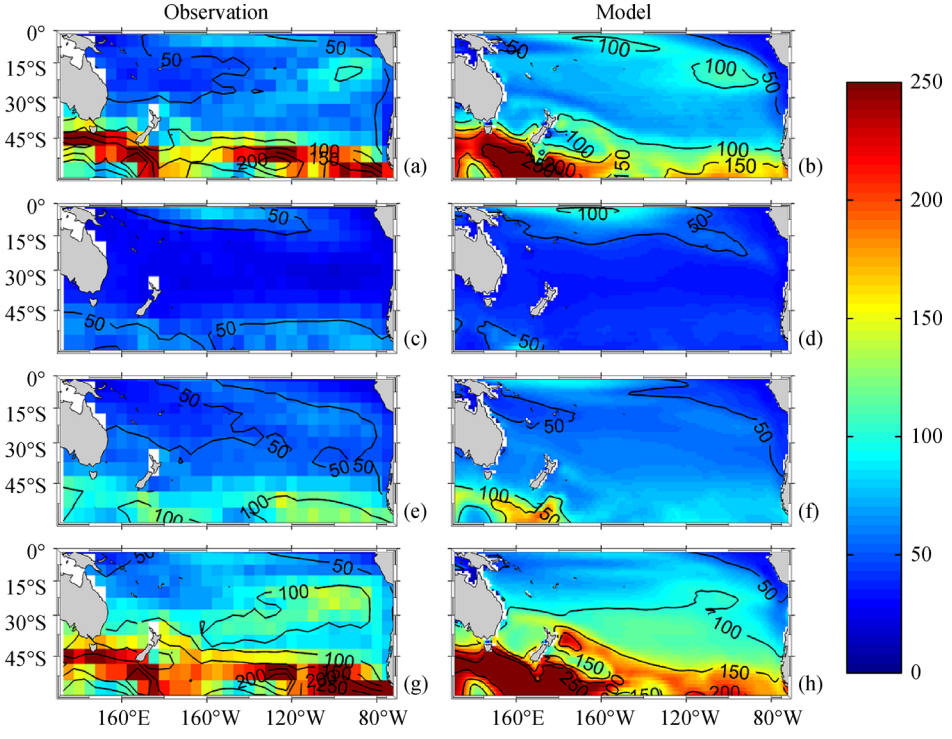

Fig. 6 Same as Fig. 2, except for the South Pacific Ocean (120°E–70°W, 0°–60°S).

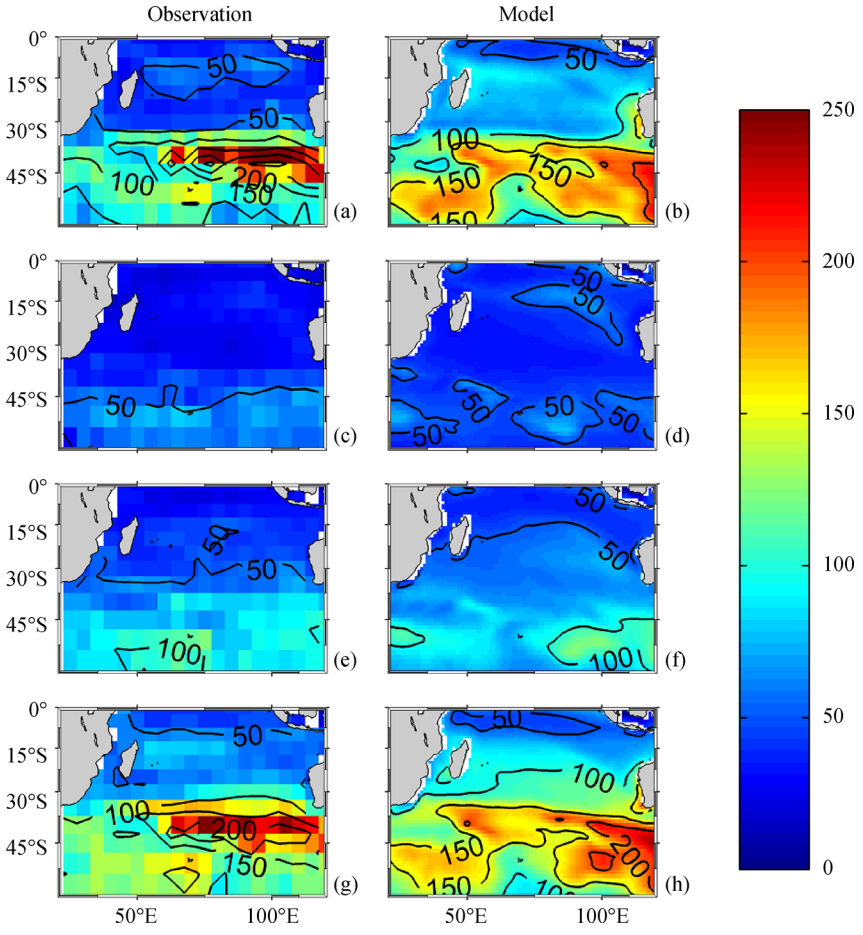

Fig. 7 Same as Fig. 2, except for the South Indian Ocean (24°–120°E, 0°–60°S).

positive". Moreover, the MLD is slightly overestimated in the west (near Uruguay) and the east (Gulf of Guinea), while it is underestimated in the central South Atlantic Ocean.

In summer, the MLD is deeper than 100 m north of 40°S and shallower than 30 m between 10°–40°S over the South Pacific Ocean (Fig. 6). The simulated MLD is similar to the observed MLD, with an area-averaged spatial correlation coefficient of 0.74. The MLD in the South Indian Ocean is shallower than that in the South Pacific Ocean north of 20°S. It is generally shallower over 10°–35°S (mostly less than 30 m) and deeper over 40°–50°S (exceeding 60 m to the west of Australia). Between 30°–60°S, the simulated MLD is slightly overestimated, and the correlation coefficient with the observation is 0.65 (Fig. 7). In the austral winter, deep MLD is found in the South Pacific Ocean and South Indian Ocean over 30°–60°S, with a maximum exceeding 250 m. In terms of spatial distribution, correlation coefficients between observed and simulated MLD are greater than 0.8 in these two oceans. Moreover, a shallow ML appears in the tropical South Indian Ocean (0°–10°S) throughout the year. Generally, the simulated ML is close to the observed in the Southern Hemisphere. Compared to other climate models (e.g., Martin, 1985; Kantha and Clayson, 1994; Ezer, 2000), which had large underestimations of the MLD in summer, the MLD here is reasonably well simulated.

3.2 Seasonal error of MLD

To further compare the simulated MLD with the observation, Figures 8−11 use scatter diagrams of the MLD in all four seasons for the six ocean regions. The simulated MLD in the Southern Hemisphere is closer to the observed than that in the Northern Hemisphere, with most simulated MLD values scattered in the vicinity of the diagonal. In the boreal fall, no large difference between observed and simulated MLD is found except for the North Indian Ocean. In the austral winter, the simulated MLD is evidently close to the observed in the South Atlantic Ocean and the South Indian Ocean, while a few values are found below the diagonal for the South Pacific Ocean.

In the Northern Hemisphere, the MLD is well simulated in the Pacific Ocean, especially with a good simulation of its spatial pattern during summer and fall (Figs. 2, 9, and 10). The scatters are concentrated along the diagonal, with

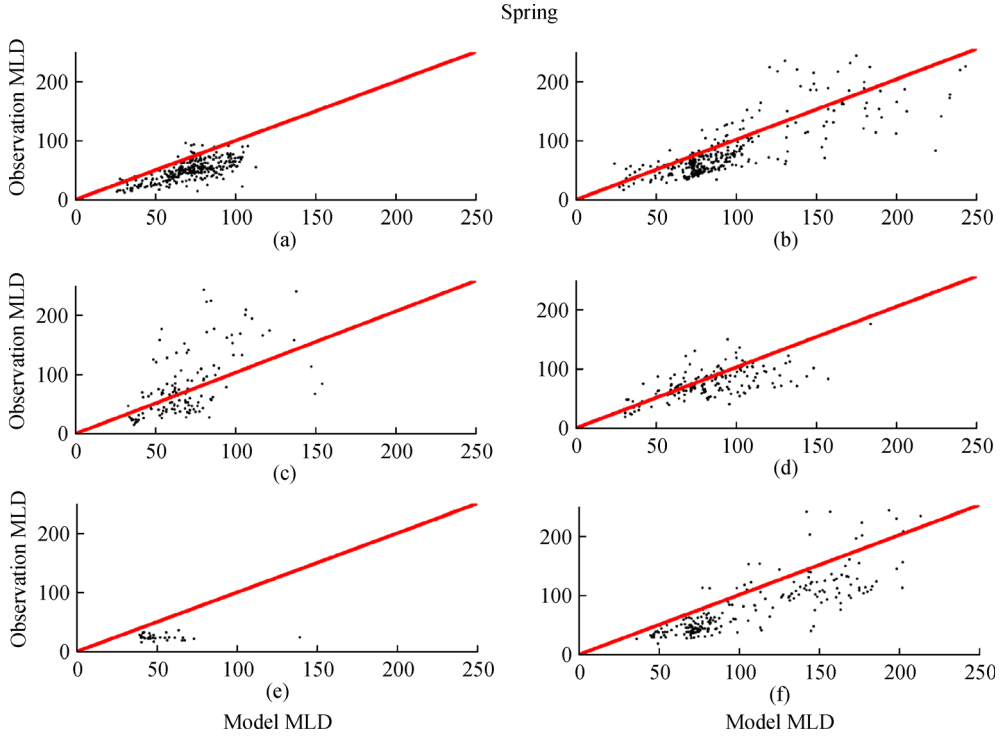

Fig. 8 Scatter diagram comparing model and observations in the six oceans in spring. (a: the North Pacific Ocean; b: the South Pacific Ocean; c: the North Atlantic Ocean; d: the South Atlantic Ocean; e: the North Indian Ocean; f: the South Indian Ocean).

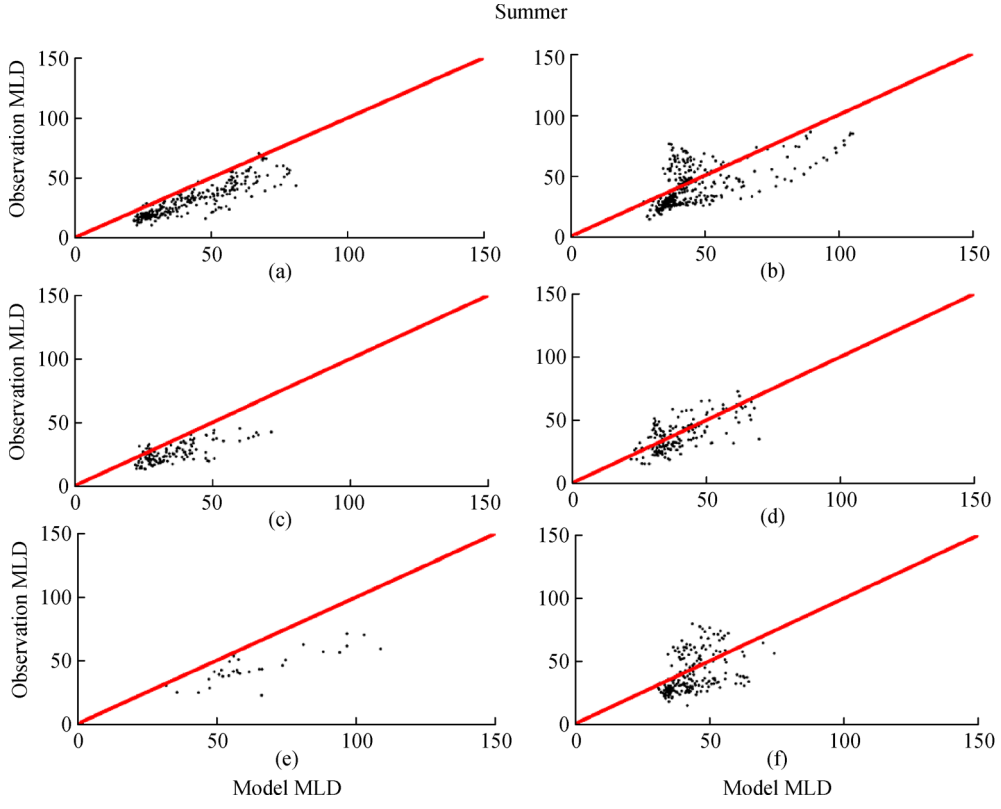

Fig. 9 Same as Fig. 8, except in summer.

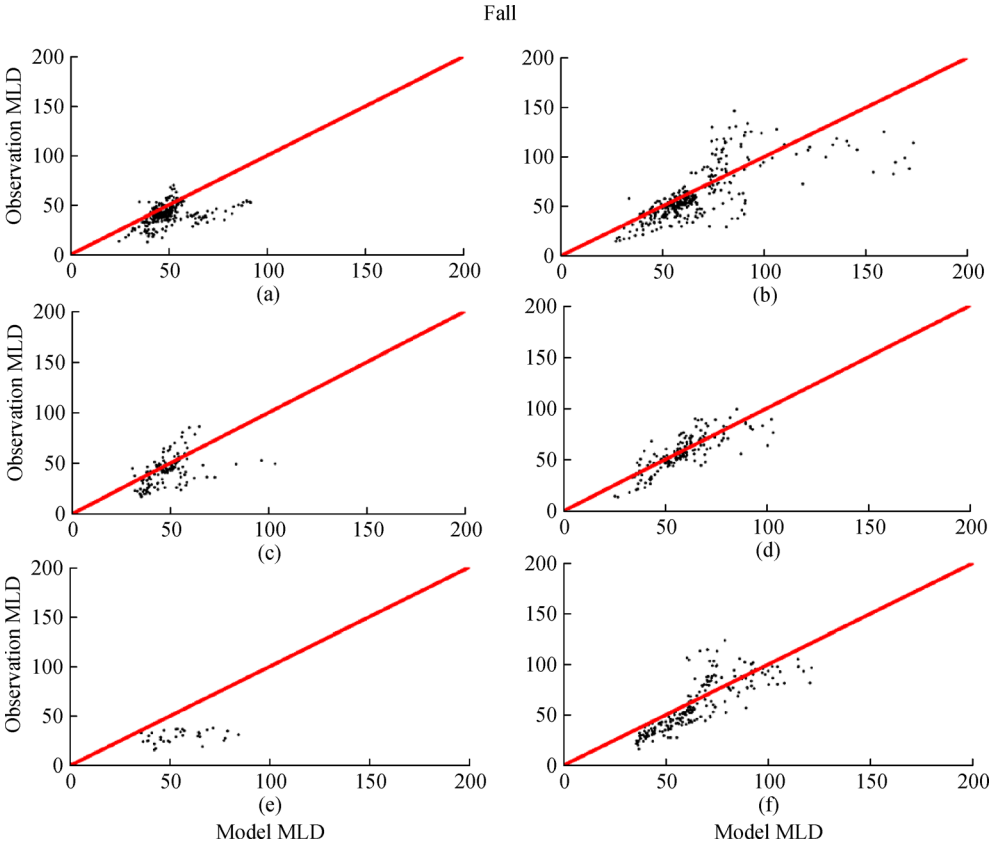

Fig. 10 Same as Fig. 8, except in fall.

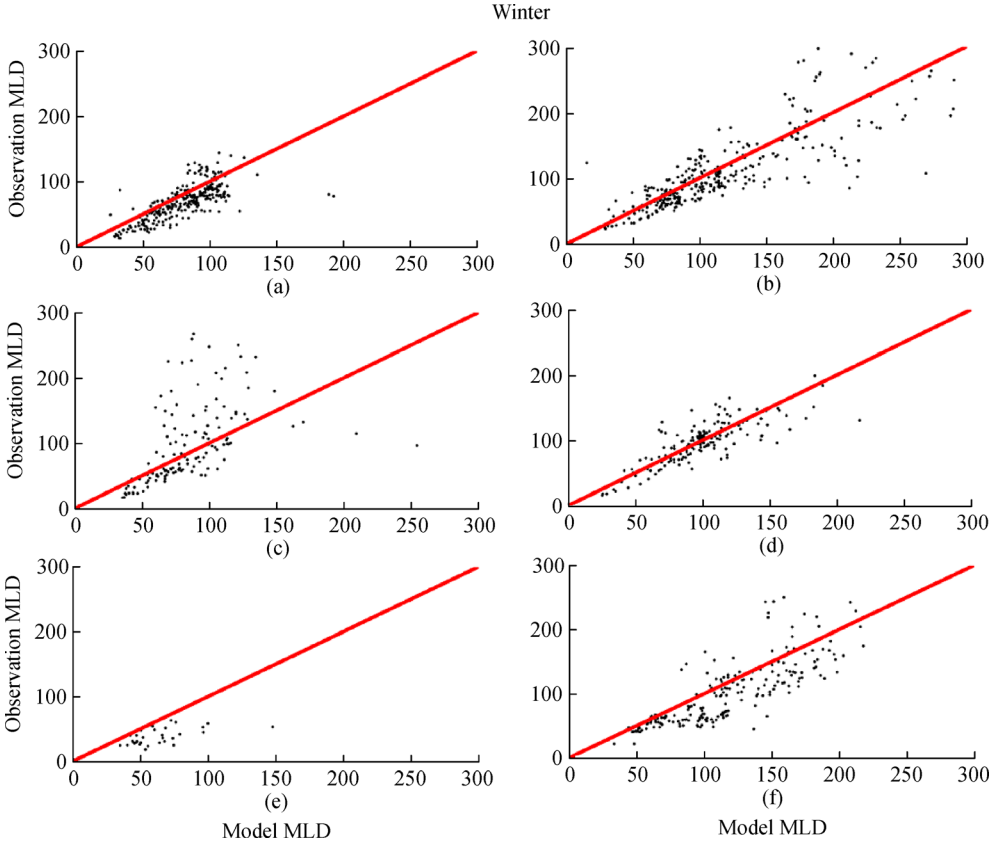

Fig. 11 Same as Fig. 8, except in winter.

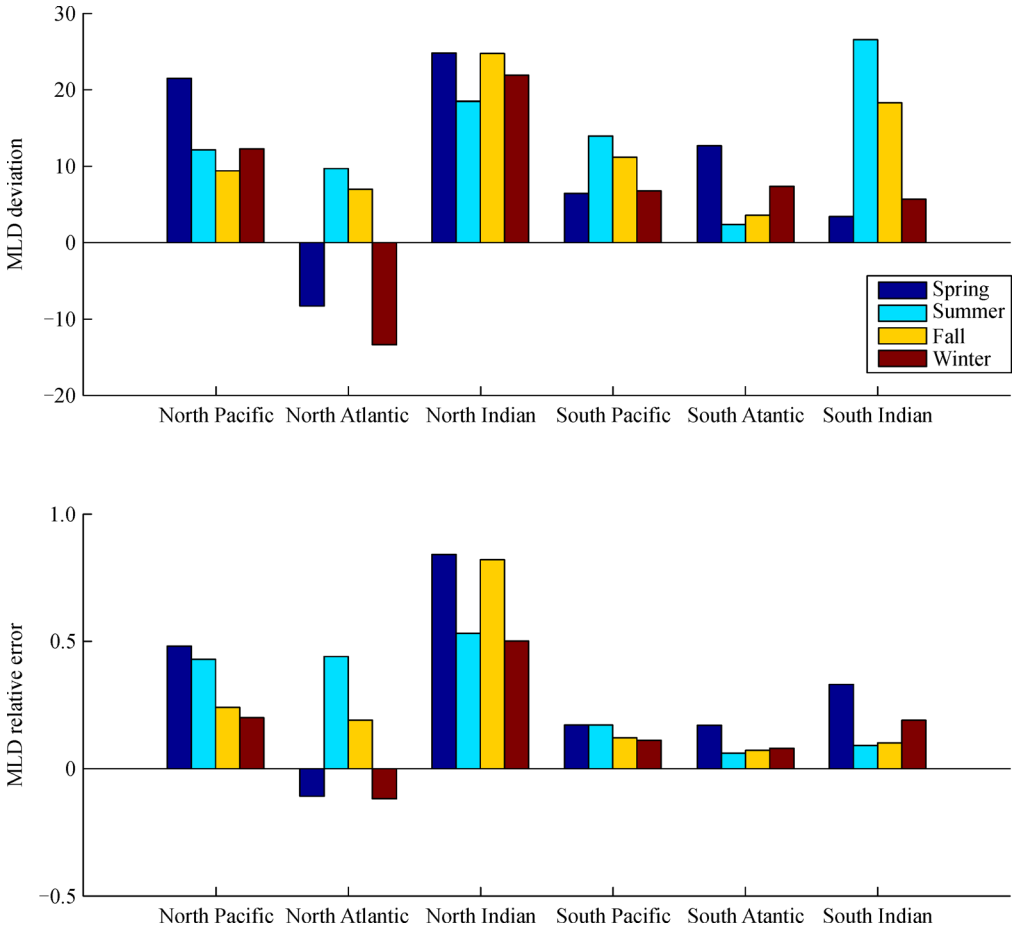

Fig. 12 Comparison of MLD deviation and relative errors in each season for the six oceans.

values smaller than 100 m. The simulation in winter is not as good as that in summer and fall, with a slightly overestimated MLD (the maximum MLD exceeding 300 m). In the North Atlantic Ocean, some scatters are located above the diagonal, especially in spring, indicating an underestimated MLD in some areas. In addition, the scatters are more dispersed during winter with the maximum reaching 400 m. In the North Indian Ocean, the model performance is worse compared to the other oceans due to the large overestimation of the MLD, with most scatters below the diagonal. In the Southern Hemisphere, the simulation in the austral summer and fall is better than that in the austral spring and winter. In the South Atlantic Ocean, most scatters are close to the diagonal, suggesting that the observed and simulated MLD are in good agreement (generally differing by less than 5 m). For the other southern oceans, slightly overestimated MLD can be seen in all seasons.

Figure 12 presents the mean deviation and relative errors of the MLD in all six ocean basins, which denotes the bias level of the model simulation. The MLD deviation and relative errors are negative during the boreal spring and winter over the North Atlantic Ocean, with values less than 20 m and 20%, respectively. This shows that the simulated MLD in spring and winter is lower than the observed, and this lower MLD is more significant in winter. The South Atlantic Ocean has the minimum deviation and relative errors in the austral summer, fall, and winter, which are less than 5 m and 10%, respectively, compared to the observation. In the North Pacific Ocean, the relative error reaches the minimum of 19.7% in winter, but exceeds 40% in summer and spring. The MLD derivation is less than 20% over the South Pacific Ocean in all seasons. The relative error is less than 10% over the South Indian Ocean in the austral summer and fall, which is close to the observation. Generally, the simulated MLD in the austral summer is closer to the observation than that in the boreal summer. However, the MLD is not well simulated over the North Indian Ocean with much larger deviation and relative error in the seasonal variation.

4 Summary and discussion

The present study evaluated the FIO-ESM performance in simulating MLD over the six main ocean basins.

Considering the importance of surface wave-induced vertical mixing in the upper ocean, the FIO-ESM introduced a surface wave model as its component. By comparing the simulated MLD with Argo observations, the following conclusions are reached.

The global ocean MLD has a strong seasonal variation with deep MLD in winter and shallow MLD in summer, due to the monsoon and the air-sea heat exchange. The spring and fall are the transitional seasons with MLD decreasing and deepening over time, respectively.

The FIO-ESM reproduced well the spatial distribution and seasonal variation of MLD over the global oceans, with much better simulation in summer and fall than in spring and winter. Among the six ocean basins, the simulated MLD in the Southern Hemisphere is much closer to the observed, probably due to the strong mixing and surface waves in the Southern Hemisphere. Although the simulated MLD is generally deeper than the observed one, the model achieves its best performance over the South Atlantic Ocean in terms of spatial pattern and relative errors in comparison with the observation. This is probably due to the fact that serious underestimation of the MLD over the South Atlantic Ocean in other climate models has been well modified after the ocean surface waves are introduced. Over the North Indian Ocean, though the simulated MLD is evidently deeper than that in the observation, the MLD spatiotemporal characteristics are consistent with observations, especially as the model captures the semi-annual cycle feature well.

The model performance in simulating MLD is further confirmed via quantitative and correlation analyses. In general, the correlation coefficient between the observed and simulated MLD exceeds 0.6 in each season of each basin. In particular, the simulated MLD agrees well with the observation in the austral fall of the South Atlantic Ocean, with the correlation coefficient exceeding statistically significant changes at the 90% confidence level.

The present study compared the FIO-ESM simulated MLD with Argo observations. We did not discuss the additional mechanisms by which the MLD varies in each ocean basin both in the model and in the observational data. More detailed analysis is under way, and we will report these results in a forthcoming publication.

Acknowledgements The present study was supported by the National Natural Science Foundation of China (Grant Nos. 41476022 and 41490643), the Startup Foundation for Introducing Talent of Nanjing University of Information Science and Technology (2013r121, 2014r072), the Program for Innovation Research and Entrepreneurship team in Jiangsu Province, and the National Programme on Global Change and Air-Sea Interaction (No. GASI-03-IPOVAI-05). Appreciation is extended to the anonymous reviewers and the editors for their valuable comments.

References

Alexander M A, Timlin M S, Scott J D (2001). Winter-to-winter recurrence of sea surface temperature, salinity and mixed layer depth anomalies. Prog Oceanogr, 49(1−4): 41–61

An Y Z, Zhang R, Wang H Z (2012). Study on calculation and spatio-temporal variations of global ocean mixed layer depth. Chin J Geophys, 55(7): 2249–2258 (in Chinese)

Collins W D, Rasch P J, Boville B A (2004). Description of the NCAR Community Atmosphere Model (CAM3.0). National Center for Atmospheric Research, tn-464 + str: tn-485 + str

de Boyer Montégut C, Gurvan M, Fischer A S (2004). Mixed layer depth over the global ocean: an examination of profile data and a profile-based climatology. Journal of Geophysical Research: Oceans, 109 (C12): C12003

Deser C, Alexander M A, Timlin M S (1996). Upper-ocean thermal variations in the North Pacific during 1970−1991. J Clim, 9(8): 1840–1855

Ezer (2000). On the seasonal mixed layer simulated by a basin-scale ocean model and the Mellor Yamada turbulence scheme. Journal of Geophysical Research: Atmospheres, 105(C7): 16843–16856

Holte J, Talley L (2009). A new algorithm for finding mixed layer depths with applications to Argo data and subantarctic mode water formation. J Atmos Ocean Technol, 26(9): 1920–1939

Huang C J, Qiao F L, Dai D (2014). Evaluating CMIP5 simulations of mixed layer depth during summer. Journal of Geophysical Research: Oceans, 119(4): 2568–2582

Huang C J, Qiao F L, Shu Q, Song Z (2012). Evaluating austral summer mixed-layer response to surface wave-induced mixing in the Southern Ocean. Journal of Geophysical Research: Oceans, 117 (C11): 24–33

Huang C J, Qiao F L, Song Z Y (2008). The effect of the wave-induced mixing on the upper ocean temperature in a climate model. Acta Oceanol Sin, 27(3): 104–111

Kantha L H, Clayson C A (1994). An improved mixed layer model for geophysical applications. Journal of Geophysical Research: Oceans, C12(99): 25235–25266

Kara A B, Rochford P A, Hurlburt H E (2000). An optimal definition for ocean mixed layer depth. J Geophys Res, D, Atmospheres, 105(C7): 16803–16821

Kara A B, Rochford P A, Hurlburt H E (2003). Mixed layer depth variability over the global ocean. Journal of Geophysical Research: Oceans, 108(C3): 3079

Kelly K A, Qiu B (1995). Heat flux estimates for the Western North Atlantic. Part I: Assimilation of satellite data into a mixed layer model. J Phys Oceanogr, 25(10): 2344–2360

Kolodziejczyk N, Reverdin G, Lazar A (2015). Interannual variability of the mixed layer winter convection and spice injection in the eastern subtropical North Atlantic. J Phys Oceanogr, 45(2): 504–525

Lu J, Qiao F L, Wei Z X (2008). Study on distributions of mixed layer depth in the world ocean in summer—Comparison between Argo data and Levitus data. Advanced in Marine Science, 26(2): 145–155 (in Chinese)

Martin P J (1985). Simulation of the mixed layer at OWS November and Papa with several models. Journal of Geophysical Research: Oceans, 90(C1): 903–916

Noh Y, Lee W S (2008). Mixed and mixing layer depths simulated by an OGCM. J Oceanogr, 64(2): 217–225

Ohno Y, Iwasaka N, Kobashi F, Sato Y (2009). Mixed layer depth

climatology of the North Pacific based on Argo observations. J Oceanogr, 65(1): 1–16

Oleson K, Niu G, Yang Z (2008). Improvements to the Community Land Model and their impact on the hydrological cycle. J Geophys Res, D, Atmospheres, 113(113): 811–827

Perry A H, Walker J M (1977). The Ocean-Atmosphere System. New York: Long-man Inc, 1–160

Prasad T G (2004). A comparison of mixed-layer dynamics between the Arabian Sea and Bay of Bengal: one-dimensional model results. J Geophys Res, D, Atmospheres, 109(C3): 325–347

Price J F, Weller R A, Pinkel R (1986). Diurnal cycling: observations and models of the upper ocean response to diurnal heating, cooling, and wind mixing. Journal of Geophysical Research: Oceans, 91(C7): 8411–8427

Qiao F L, Huang C J (2012). Comparison between vertical shear mixing and surface wave-induced mixing in the extratropical ocean. Journal of Geophysical Research: Oceans, 117(C11): C00J16

Qiao F L, Song Z Y, Bao Y (2013). Development and evaluation of an Earth System Model with surface gravity waves. Journal of Geophysical Research: Oceans, 118(9): 4514–4524

Qiao F L, Yang Y, Xia C (2008). The role of surface waves in the ocean mixed layer. Marine Journal: English edition, 18(3): 30–37

Qiao F, Yuan Y, Yang Y, Zheng Q, Xia C, Ma J (2004). Wave-induced mixing in the upper ocean: distribution and application to a global ocean circulation model. Geophys Res Lett, 31(11): 293–317

Shu Q, Qiao F L, Song Z Y (2013). The hindcast and forcast of Arctic sea ice from FIO-ESM. Acta Oceanol Sin, 35(5): 37–45

Smith R, Jones P, Briegleb B (2010). The Parallel Ocean Program (POP) reference manual. Los Alamos National Laboratory, LAUR-10-01853

Song Z Y, Qiao F L, Wang C (2011). The correctness to the spuriously simulated semi-annual cycle of the sea surface temperature in the equatorial eastern Pacific. Sci China Earth Sci, 54(3): 438–444

Song Z Y, Qiao F L, Yang Y Z (2007). An improvement of the too cold tongue in the tropical Pacific with the development of an ocean-wave-atmosphere coupled numerical model. Prog Nat Sci, 17(5): 576–583

Sprintall J, Roemmich D (1999). Characterizing the structure of the surface layer in the Pacific Ocean. Journal of Geophysical Research: Oceans, 104(C10): 23297–23311

Sprintall J, Tomczak M (1992). Evidence of the barrier layer in the surface layer of the tropics. J Geophys Res, D, Atmospheres, 97(C5): 7305–7316

Thomson R E, Fine I V (2010). Estimating mixed layer depth from oceanic profile data. J Atmos Ocean Technol, 20(20): 319–329

Yang Y Z, Qiao F L, Zhao W (2005). MASNUM ocean wave numerical model in spherical coordinates and its application. Acta Oceanol Sin, 27(2): 1–7